J Mater Sci (2009) 44:2226–2238
DOI 10.1007/s10853-008-3076-1

FESTSCHRIFT IN HONOUR OF PROF T R ANANTHARAMAN ON THE OCCASION OF HIS 80TH BIRTHDAY

Grain boundary sliding controlled flow and its relevance to superplasticity in metals, alloys, ceramics and intermetallics and strain-rate dependent flow in nanostructured materials

K. A. Padmanabhan

Received: 2 May 2008 / Accepted: 21 October 2008 / Published online: 23 November 2008

Abstract A model that was proposed originally to account for optimal superplasticity in metals and alloys with grain size in the micrometer range and later extended in a few subsequent papers to cover optimal superplastic deformation in ceramics, sub-micrometer-grained and nanostructured materials and intermetallics is described, with an emphasis on the current ideas used in this model and the mathematical procedure used at present (yet to be published in detail) for validating the proposals. The central assumption is that the rate controlling deformation process is confined to high-angle grain/interphase boundary regions that are essential for grain boundary sliding developing to a mesoscopic scale (defined to be of the order of a grain diameter or more) and for superplastic flow setting in. The strain rate equation was validated against experimental observations concerning metals, alloys and ceramics of micrometer- and sub-micrometer grain sizes, nanostructured materials and intermetallics.

Introduction

Of the two types of superplasticity [1–3], (a) environmental/transformation superplasticity and (b) structural superplasticity, only the latter will be considered in this paper. Structural superplasticity has been reported in metals and alloys, intermetallics and ceramics. When the grain size is in the sub-micrometer range, "high-strain rate" superplasticity (strain rate of deformation, $\dot{\varepsilon} \geq 10^{-2}$ s^{-1}) and "positive index strain rate" superplasticity ($\dot{\varepsilon} \geq 10^{0} = 1$ s^{-1}) are encountered. Extreme (superplastic) elongations have also been reported in bulk metallic glasses and hot inorganic glasses. Even in very early works, the similarity between the deformation behavior of superplastic alloys and tar, pitch, "silly putty", plasticine and "chewing gum" was noticed. More recently, nanocrystalline materials have been rendered superplastic. In the class of metals and alloys, crystal structure has negligible effect on superplastic behavior; alloys that have FCC, BCC or HCP structures are all significantly superplastic. Intermetallics, in which movement of dislocations is rather difficult, also display a superplastic response very similar to that of metallic materials. Therefore, in our opinion it is desirable to describe the phenomenon of superplastic flow invoking only those microstructural features that are common to all the above-mentioned classes of materials.

A survey of literature

As the phenomenon of structural superplasticity has been established in different classes of materials, the field has remained active. A quick search of literature reveals that 234 papers have been published on superplasticity and superplastic forming since the beginning of year 2000. It is not possible to review all these papers in detail in a short publication. Therefore, the new directions in research and some of the more recent findings/conclusions are recorded.

Much finer grain sizes have been produced using different techniques. Severe plastic deformation (SPD) through the use of high-pressure torsion (HPT) [4–10],

This paper is dedicated to Prof. T. R. Anantharaman, who celebrated his 80th birthday recently.

K. A. Padmanabhan (✉)
Department of Mechanical Engineering, Materials Science and Engineering Division, Anna University, Chennai 600 025, India
e-mail: ananthaster@gmail.com; kap@annauniv.edu

equi-channel angular pressing/processing (ECAP) [11–18], equi-channel angular extrusion (ECAE) [19], friction stir processing [20, 21], differential rolling (single pass rolling, with a high speed ratio) [22], normal multi-pass rolling [23, 24], pulse electrodeposition [25] and electromagnetic casting, accompanied by electromagnetic stirring [26], are the different methods used. The grain size range has varied from 1 to 3 μm down to a few tens of nanometer. The HPT and pulse electrodeposition techniques have been the most effective in reducing the grain size into the nanometer range. The need to ensure a homogeneous, ultra-fine grain size in fairly large samples has been understood. The degree of success has depended on the efficacy of the processing route and the composition of the material. When ECAP was used, ductility increased when the resultant microstructure consisted of a homogeneous array of grains, separated by high-angle boundaries [12, 13]. In addition, the maximum ductility obtainable was decided by the sub-classification within ECAP adopted [12, 13]. Superplastic elongation increased as one went from an as-cast to cast and extruded to cast, extruded and ECAPed microstructure [13]. After a HPT treatment, the microstructure was inhomogeneous and the grain size changed with the location in the sample. This, in turn, affected the extent of superplastic behavior [9]. Mg–9wt.%Al alloy, which could not be processed easily by ECAP, could be rendered superplastic using the HPT technique [10].

The above-mentioned investigations were carried out on a variety of materials, viz., alloy Ti–6Al–4V [4, 7], Al 1420 [5], Cu–40%Zn [11], Al–3Cu–0.2Sc [12, 13], Cu–38Zn–3Sn [14], Al–Mg–Sc–Zr alloys [15, 17], Al 2024 [27], ZK 60 Mg alloy [19, 28], an Al–Mg–Sc alloy [9], Mg–8Li and Mg–9Al alloys [10, 13], nanostructured Ni [25], AZ 91 Mg alloy [23, 24], Mg alloy AZ 61 [22], Al–Li alloy AA 8090 [29], several Al–Ti alloys [30], Zr-modified Al 2014 and AM 60 B Mg alloys [20, 21], Al–5.7Mg–0.3Sc–0.3Mn [18], Mg alloys and composites made through powder metallurgy and ingot metallurgy routes [31], Ni_3 Al [4, 5], ceramic intermetallic composite Ti_5 Si_3 plus 40 vol.% Ti Al [32], ZrO_2/Ni nanocomposite [25], oxide ceramics [33], ZrO_2–spinel composite [34], alumina dispersed with 3 mol.% yttria-stabilized zirconia or magnesia [33, 35], nanostructured Si_3N_4 [36], 2–3 mol.% yttria partially stabilized zirconia [27, 36, 37], Al 2014 matrix reinforced with TiC particles [38], β-Si_3N_4 with 5 wt.% yttria and 22 wt.% magnesia [39], and Zirconia–3 mol.% yttria–alumina–alumina–magnesia spinel nanoceramic composite [40].

The major conclusions that have been drawn are as follows. (a) When the grain size is reduced into the range 1–3 μm to a few tens of nanometer, superplastic deformation is present at a higher strain rate and/or a lower temperature [4, 7, 11, 15, 16, 18, 22, 24, 27, 32, 40]. This is in line with what is known since the 1960s. (b) In ECAPed Cu alloys internal cavitation is present during superplastic flow, as during conventional superplasticity in this class of alloys [14]. (c) For high strain rate superplasticity in oxide ceramics, a fine grain size, enhanced diffusivity, restricted dynamic grain growth, a homogeneous microstructure and reduced residual stresses should all be present simultaneously [33]. (d) The presence of high-angle boundaries is essential for superplastic deformation [28] and when low-angle boundaries are present, they are gradually eliminated with increasing superplastic strain [17]. (e) At a given temperature, the stress exponent, n, changes significantly with stress [36]. (f) The threshold stress needed for the commencement of superplastic flow decreases with increasing temperature [41]. (g) Superplastic flow characteristics of a material of a fixed average grain size change significantly when the grain size distribution and the number and distribution of large grains are different [42]. (h) Grain boundary sliding is the deformation mechanism and not just an accommodation mechanism during superplastic flow [43]. (i) Both strain and strain rate hardening are simultaneously present during superplastic flow in nanostructured materials [4–7, 40]. Barring the last observation, all the other conclusions are in accordance with what is already known for a long time on steady state, optimal (conventional) superplastic flow. The last observation, in our opinion, is the result of the temperature of deformation being in a range lower than the optimal. Such a situation can be handled in a straightforward manner in mechanics (see pp. 20–23 of Ref. [1]) by starting with a constitutive equation that includes both strain and strain rate hardening. But a physical mechanism involving both strain hardening and strain-rate hardening is yet to be developed.

No new/unexpected conclusions with regard to the operating physical mechanisms have been drawn. Some important conclusions are (a) co-operative grain boundary sliding [44, 45], which has also been described as 'recombinant domain movement' [46], is responsible for superplastic flow. (b) The view [37, 47–49] that superplastic flow in yttria-stabilized zirconia is due to grain boundary diffusion creep (Coble creep), which changes to interface-controlled creep at lower stresses, has been questioned and an alternative view is expressed that grain boundary sliding is not just an accommodation mechanism, but it is the deformation mechanism [27, 43].

It is pertinent to note at this stage that the phenomenon of superplasticity has already been defined in mechanics on a common basis, which applies to all the classes of materials listed above, viz., "superplastics are materials whose mechanical response during steady state (stationary) uniaxial tensile deformation can be described by the power law $\sigma = K\dot{\varepsilon}^m$, with $m \geq 0.3$, where σ is the steady-state

stress, $\dot{\varepsilon}$ the corresponding strain rate, K a constant and m is the strain-rate sensitivity index" [50].

A majority of workers in the area of superplasticity in materials of grain size in the micrometer and sub-micrometer range use

$$\dot{\varepsilon} = A\left(\frac{D_0 Gb}{kT}\right)\left(\frac{b}{d}\right)^p\left(\frac{\sigma}{G}\right)^n \exp\left(\frac{-Q}{RT}\right) \quad (1)$$

as a generic equation to account for elevated temperature plasticity/steady state creep rate, where $\dot{\varepsilon}$ is the steady state creep rate, G the shear modulus, b the Burgers vector, A a constant, $D_0 \exp(\frac{-Q}{RT})(=D)$ is the appropriate diffusion coefficient, with D_0 a frequency factor, Q the activation energy for the rate-controlling process, R the gas constant, d the grain size, k the Boltzmann constant, T the temperature of deformation on the absolute scale, σ the flow stress and p and n are constants (for the latest views on this approach, see Refs. [51, 52]). Present author has refrained from using this approach because he sees good sense in what is stated in Refs. [53–56] concerning the use of this equation even for the relatively simple case of high-temperature creep (where stress independence of n and very limited/negligible grain size dependence of $\dot{\varepsilon}$ are present). (a) Physics behind the constants A and n is not clear. (b) In different systems, n and A vary widely and A is far from being a constant. (c) A and n are not independent of each other, but are linearly related in a unique manner (and so they cannot be determined independent of each other, as suggested in Ref. [54]). (d) There is "great advantage" in normalizing the stress with respect to the tensile yield stress (as done by the engineers), instead of the shear modulus. (G then will appear as a separate variable, expressed in a dimensionless form, that affects the flow rate.) (e) Finally, the correlation between A and n can be understood without reference to any physical mechanism [56], because experimentally the majority of creep data lies in the range

$$10^{-4} < \frac{\sigma}{G} < 10^{-3};\ 10^{-14} < \frac{\dot{\varepsilon}kT}{DGb} < 10^{-8}$$

which is an extremely small range in the normalized (σ/G) space.

In this paper, it is suggested that a physical mechanism originally proposed to understand optimal superplasticity in micrometer-grained metallic alloys and later refined to include some more classes of materials can be used to understand the superplastic response of the different classes of materials listed above on a common basis. A recently developed mathematical procedure that allows the validation of the model without using any adjustable constants/parameters will also be described briefly. This way the different details of this model, scattered in different papers, will be brought together in a single publication. Unlike in the earlier papers, the focus will be on the physical concepts used, keeping mathematical treatment to a minimum level.

The model

Assumption and its justification

It is assumed that during the occurrence of structural superplasticity, the rate-controlling process is confined to the grain/interphase boundary regions and that grain deformation in the vicinity of grain boundaries, by dislocation/partial dislocation emission and diffusion, needed to ensure the continuity of strain across grains and coherence of deformation, is a faster accommodation process.

This view, when expressed first [57–59], was not in agreement with the opinion of most other workers in the field, who believed that grain boundary sliding is an inherently fast process, and that at no stage of superplastic flow it could be rate controlling. Most of the models for superplastic deformation presented at that time were based on either dislocation- or diffusion-controlled flow processes. But the observation of superplastic flow in nanostructured and bulk amorphous materials has made the dislocation-rate controlled mechanisms less attractive as a general description of deformation in different classes of superplastic materials.

There is overwhelming experimental evidence that grain boundary sliding is the dominant mechanism of deformation when superplasticity is present. There is also clear evidence for limited amounts of diffusional and dislocation activity [1–3]. Many authors have tried to combine these three different mechanisms in different proportions to predict the observed steady state, isothermal strain rate versus stress sigmoidal curve. By a mathematical examination of this additive procedure, it has been shown [50] that physical models based on the hypothesis that the effects of the three mechanisms of grain boundary sliding (GBS), diffusion creep (DC) and intragrannular slip (IS) are additive, i.e.,

$$\dot{\varepsilon}_{\text{total}} = \dot{\varepsilon}_{\text{GBS}} + \dot{\varepsilon}_{\text{DC}} + \dot{\varepsilon}_{\text{IS}} \quad (2)$$

cannot account for the sigmoidal curve seen during superplastic flow, regardless of the proportions in which they are combined. So, the overall strain rate equation has to be obtained by considering other ways of combining the individual mechanisms.

Evidence for dislocation activity has been obtained using TEM. But this technique cannot reveal whether dislocation motion in the grain interior contributes independently to superplasticity or not. In contrast, a study of the changes in the texture of an alloy due to superplastic

deformation can reveal this and it is shown later that there is no independent contribution from dislocation motion to superplastic flow. Therefore, there is a case to suggest that optimal superplastic flow rate is the result of the combined operation of grain boundary sliding and diffusional flow. However, the physical description should also involve dislocation activity, albeit in a non-rate controlling manner, if the model is to be consistent with the microstructural observations concerning dislocation/partial dislocation (which will depend on the grain size) activity in the vicinity of the grain boundary. But the two mechanisms (GBS and DC) are inter-dependent and one may refer to them together as "diffusion accommodated grain boundary sliding" or "diffusion creep, accommodated by grain boundary sliding". As a result, one may attribute the externally observed strain rate either to a diffusion mechanism or grain boundary sliding, with the other mechanism being considered the faster process and so not a part of the rate equation [60, 61]. Each assumption has its predictions with regard to the microstructural changes that will accompany superplastic flow. The amounts of strain contributed by each of the two mechanisms to the external strain will also change within limits with the mechanism selected as the rate-controlling process [62, 63].

Models based on these two assumptions, viz., diffusion creep is rate controlling [64] or grain boundary sliding is rate controlling [59, 65–72], are available. In the latter view, grain boundary sliding is regarded as a two scale process, i.e., at the level of the atomistics, the initial relative displacement of one grain with respect to its neighbor along their common boundary is considered and in the next level, the development of this boundary sliding process to a mesoscopic scale (defined to be of the order of a grain diameter or more) by the formation of plane interfaces is described (see later for details). Such plane interfaces, which can form simultaneously in different regions of the deforming specimen, can interconnect. Then, large-scale boundary sliding and significant specimen elongation can result. This description, originally presented in Ref. [73], was reproduced in Refs. [66–68], which were submitted for publication around the same time—for example, see Fig. 1 of Ref. [66]. In this picture the regions hatched indicate the regions to which the rate-controlling mechanism is confined in three dimensions. The grain shapes considered were tetrakaidecahedron (the Kelvin solid), which has been suggested as the ideal shape of the grains, and rhombic dodecahedron, the shape real grains resemble the closest [74].

When the nature of the grain boundaries that promote superplasticity was examined, it became clear that high-angle grain boundaries are very conducive to superplastic flow. As mentioned earlier, low-angle boundaries, when present, transformed into high-angle grain boundaries with increasing superplastic strain. Although it was known for quite some time from bi-crystal experiments that the extent of boundary sliding is significantly greater in general/random high-angle boundaries than in low-angle as well as low sigma, albeit at high-angle boundaries [75], extrapolation of this result to interpret superplastic deformation in polycrystalline materials is not straightforward. But this point was driven home forcefully during the development of Al–Li superplastic alloys that when the grain boundaries are of the low-angle type, no superplasticity is observed, but the same alloys become significantly superplastic when the grain boundaries are converted into the high-angle type by a change in the processing route [3, 76].

When Ref. [59] was submitted for publication, the only description of high-angle grain boundaries available was based on an extension of the CSL model for low-angle grain boundaries [77, 78] to the former type also using more and more misfit dislocations, based on an empirical (experimental) suggestion [79]. A scholarly review of the late 1970s of this approach is available [80]. As noted in that paper [80], the question whether most high-angle boundaries have structure is difficult to resolve from experiment because of inadequate statistics, but it is very relevant to dynamic observations, e.g., the absorption of lattice dislocations into grain boundaries. In some cases [81, 82], the dislocation image gradually becomes fainter and disappears and this has been explained in terms of splitting of dislocation, spreading and overlap of dislocation cores. The theoretical justification is provided by the argument that when there is no long-range order, as in general high-angle boundaries and metallic glasses, at infinite time the shear modulus falls off to zero. (Definition of an amorphous material/liquid is that it cannot support a shear stress.) Then, from the Peierls–Nabarro equation, it follows that the width of the dislocation (defined by its core) becomes infinite (see Eqs. 5–9 of Ref. [83]). To the best of our knowledge, MD simulations also have provided no evidence for the glide of grain boundary dislocations along high-angle boundaries. An alternative view was also presented that in some cases the dislocation dissociates into DSC (displace-shift-coincide) dislocations with Burgers vectors too small to be observable [84] but it does not seem to have been followed up. It is significant that all descriptions of high-angle boundaries since 1977 [85–96] describe the regions of misfit, i.e., the "bad crystal" part in high-angle boundaries, in terms of a free volume. Our approach is consistent with all these later descriptions [85–96]. It is well known that for understanding the mechanical response of materials the description of the regions of misfit, e.g., regions containing dislocations in the crystal lattice, the 'bad crystal' part in high-angle grain boundaries, is of the essence because it is in these regions of misfit that plastic deformation originates and then spreads

throughout the material along paths of lowest resistance (principle of minimum work).

Moreover, it has been demonstrated that in high-angle grain boundaries the free volume varies only slightly with misorientation and that the excess volume due to the expansion present is $\simeq 0.1\ \Omega$, where Ω is the atomic volume in the lattice [96]. This finding, coupled to the present approach, allows the development of a deterministic model of grain boundary sliding, as a first order approximation, because the excess free volume present at the high-angle grain boundary is then independent of boundary misorientation (see section "Conclusion remarks" also) and will have a mean value of 0.1 Ω.

The analysis

In this approach [65–72], every high-angle boundary, conducive to boundary sliding, is divided into a number of atomic scale ensembles that surround free volume sites present at discrete locations characteristic of the boundary. High-angle grain boundaries, except the low sigma types [75, 76], will contribute significantly to boundary sliding and superplasticity, albeit at different rates, depending on (a) the degree of "openness" of their structure and (b) their orientation with respect to the stress direction. Therefore, grain boundary sliding gives rise to an internal stress distribution/re-distribution, which will depend on the parameters of deformation in the neighborhood and hence is a function of time [66].

For mathematical development, the shape of the basic sliding unit is assumed to be an oblate spheroid of about 5 atomic diameter size in the boundary plane and 2.5 atomic diameter in the perpendicular direction, with the ensemble being located symmetrically about the plane of the boundary with one half falling in each of the two grains that meet to form the boundary. The oblate spheroid shape was chosen because the stress–strain field that will develop when such a shape is deformed has already been worked out [97]. The very small dimensions chosen will localize the stresses and make them of short range. The presence of free volume will make the basic sliding unit weaker than the rest of the boundary. The average shear strain associated with a unit sliding event when the ensemble moves from one metastable position to the next is calculated by assuming the grain boundary to be 3 atomic diameter thick [66, 98, 99]. Using the results of Ref. [96], this mean shear strain is equated to 0.10. When this shear process spreads consecutively to the end of the boundary, an externally measurable grain boundary sliding displacement results. The elastic energy of the shear and volumetric distortions accompanying the unit-shear, ΔF_0, constitutes the activation energy for the grain boundary sliding process.

The (momentary) volumetric dilatation arises from the fact that the oblate spheroid is embedded in a solid matrix. Following Ref. [97], for the oblate spheroid shape assumed, the free energy of activation for the boundary sliding process, ΔF_0, is estimated as

$$\Delta F_0 = \frac{1}{2}\left(\beta_1 \gamma_0^2 + \beta_2 \varepsilon_0^2\right) G V_0 \tag{3}$$

$\beta_1 = 0.944\left(\frac{1.590-p}{1-p}\right)$; $\beta_2 = \frac{4(1+p)}{9(1-p)}$; p is Poisson's ratio, γ_0 the mean shear strain associated with a unit-sliding event ($\simeq 0.1$), ε_0 the normal/dilatational strain associated with the same event ($= \frac{\gamma_0}{\sqrt{3}}$; from von Mises relationship), G the shear modulus of the high-angle boundary region under consideration and V_0 is the volume of the sliding unit (oblate spheroid) $= \frac{2}{3}\pi(2.5a_0)^3 = \frac{2}{3}\pi W^3$, with a_0 the atomic diameter and W the width of the grain boundary in both micrometer- and nanometer-grained materials, on average equal to about $2.5a_0$ [98, 99].

But after sliding for a length of the order of a grain diameter/side, a triple junction is in the way and this will terminate the relative motion between the grains. Thus, steric hindrance renders this kind of boundary sliding rather limited.

In order to produce substantial sliding on a mesoscopic scale, two or more grains must align to form a plane interface, which by further interconnection with other similar plane interfaces will lead to long range sliding before it gets stopped at an insurmountable barrier, e.g., an extra large grain, a coarse precipitate. In forming the plane interface, grain boundary energy must be spent which is supplied by the external stress. This gives rise to a long-range threshold stress that has to be overcome by the external stress before mesoscopic boundary sliding can set in. The driving force for such a plane interface formation arises from (a) the minimization of the total free energy of the deforming system and (b) the work done by the external stress reaching its maximum value for this configuration (the plane interface)—principle of maximum work [66, 71].

The long-range threshold stress that should be overcome for forming the plane interface is calculated by describing the polycrystalline structure as a cubic dense packing of equi-sized spheres. The walls of the Wigner–Seitz cell containing one sphere represent the grain boundaries. This corresponds to a face-centered cubic structure on a mesoscopic scale with glide planes and glide directions. Since the roughness is the least on the {111} planes, they are assumed to be the glide planes for long-range boundary sliding. The surface of a {111} plane in the mesoscopic structure consists of a regular arrangement of peaks and troughs whose height, h, will vary as L, the average grain size. Likewise, the ground area, A, will vary as L^2, regardless of grain shape. In order to create a plane

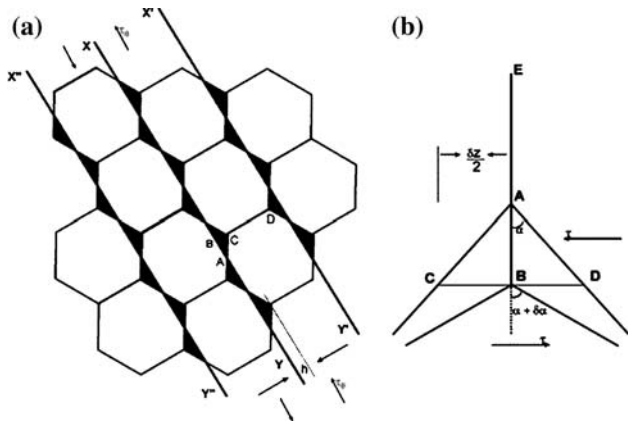

Fig. 1 **a** A 2D section of grains of equal size. Planar interfaces along XY, $X'Y'$, $X''Y''$ etc. result if the atoms located in the dark regions, e.g., in region ABC, move by non-rate controlling dislocation emission/diffusion to the boundaries that are normal to the direction of the externally applied shear stress, e.g., boundary CD. **b** Shear stress-driven movement of a boundary triple junction, A. The triple junction is formed by three boundaries: AC, AD and AE. If an external stress, τ, is applied, as indicated, the resulting internal stresses in the vicinity of the triple junction will be reduced when the triple junction migrates from position A to position B (both (**a**) and (**b**) after Ref. [71])

interface, the peaks and troughs of the mesoscopic {111} plane must be leveled, i.e., the grain boundary area in the mesoscopic glide plane should be decreased by local boundary migration. A 2D section of the three-dimensional microstructure would appear as in Fig. 1a. The shaded portions are the 2D sections of the peaks and valleys that should be leveled by local boundary migration for plane interface formation. In Fig. 1b, external shear stress-driven movement of a boundary triple junction is shown. The internal stresses in the vicinity of the triple junction are reduced by the migration of point A to point B, i.e., when the semi-angle of the triple junction, α, increases with increasing external shear stress. It can be shown that in the limit $\alpha \rightarrow 90°$, i.e., the plane interface is formed [71]. Evidently, such a process is considerably easier than diffusion by either Nabarro–Herring or Coble creep. The magnitude of the threshold stress, which should be overcome before the plane interface can be formed, is calculated by an energy balance. In mechanistic terms, in the general case the peaks and troughs are leveled first by the non-rate controlling emission of dislocations from the projecting grain boundary corner in a barrier-free manner or during a thermal event. This will happen when (a) the misfit in the local region of the (high-angle) boundary increases by the atomic scale sliding process described earlier to equal the Burgers vector of a unit dislocation (which could be replaced by a partial dislocation, when the grain size is in the lower end of the nanometer scale) that can be emitted into one of the two grains that form the grain boundary of an appropriate orientation, and (b) the stress developed as a result of atomic scale sliding and the accumulated local misfit equals the stress necessary to trigger the emission of the dislocation/partial dislocation into the grain concerned [66, 100]. The remaining misfit, which may not be an integral multiple of the Burgers vector of the dislocations being emitted, will be removed by diffusion. Scope exists for analyzing this problem using MD simulations in the future by considering high-angle grain boundaries of different misorientations. More importantly, as in this process only the re-shaping of the grain corners is involved, there will only be a very limited change in the grain shape, as required by the experimental results. Also, this process will not be self-exhausting, as is the case with the N–H and Coble creep models [1]. These theoretically predicted plane interfaces were indeed observed using TEM in both micrometer-grained and nanometer-grained materials (Fig. 2a, b).[1]

It may be argued that a majority of researchers in the area of superplasticity in micrometer- and sub-micrometer-grained crystalline solids maintain that grain boundary sliding provides the major component of strain but that the accommodation process to handle the stresses generated at triple junctions due to grain boundary sliding is accomplished by dislocation plasticity. It has already been pointed out in the section "Assumption and its justification" that such a description, which involves the glide of grain boundary dislocations along high-angle grain boundaries (see, e.g., Refs. [101–104]), is not consistent with any of the models for general high-angle boundaries proposed since 1977 [85–96], in all of which the misfit/expansion present in such boundaries is described in terms of a free volume. This was one of the reasons why we did not consider deformation by dislocation plasticity inside the grains or in the grain boundaries as a concomitant of the rate-controlling process. The picture becomes clearer in the nanometer-grain size range because, to the best of our knowledge, in none of the MD simulation results (or high-resolution TEM pictures corresponding to micrometer-, sub-micrometer or nano-grained materials) presented to date there is evidence for the glide of grain boundary dislocations along the grain boundaries.

[1] To the best of our knowledge, the first experimental observation using TEM of plane interface formation in any superplastic, alloy was reported in Ref. [123]. As this feature is visible more clearly in Ref. [122], that picture is reproduced here. Very recently, plane interface formation in a nanometer-grained intermetallic was illustrated in Refs. [101, 124] using TEM. Starting from early 1990s, many papers from the groups of Kaibyshev, Mukherjee, Baudelet and Ovid'ko have appeared, in which "cooperative grain boundary sliding" is illustrated using SEM. Evidently, the resolution in those micrographs is not high enough to decide if the deformation is confined to the grain boundary regions only or grain interior adjacent to the grain boundary regions also is involved in the rate controlling deformation process.

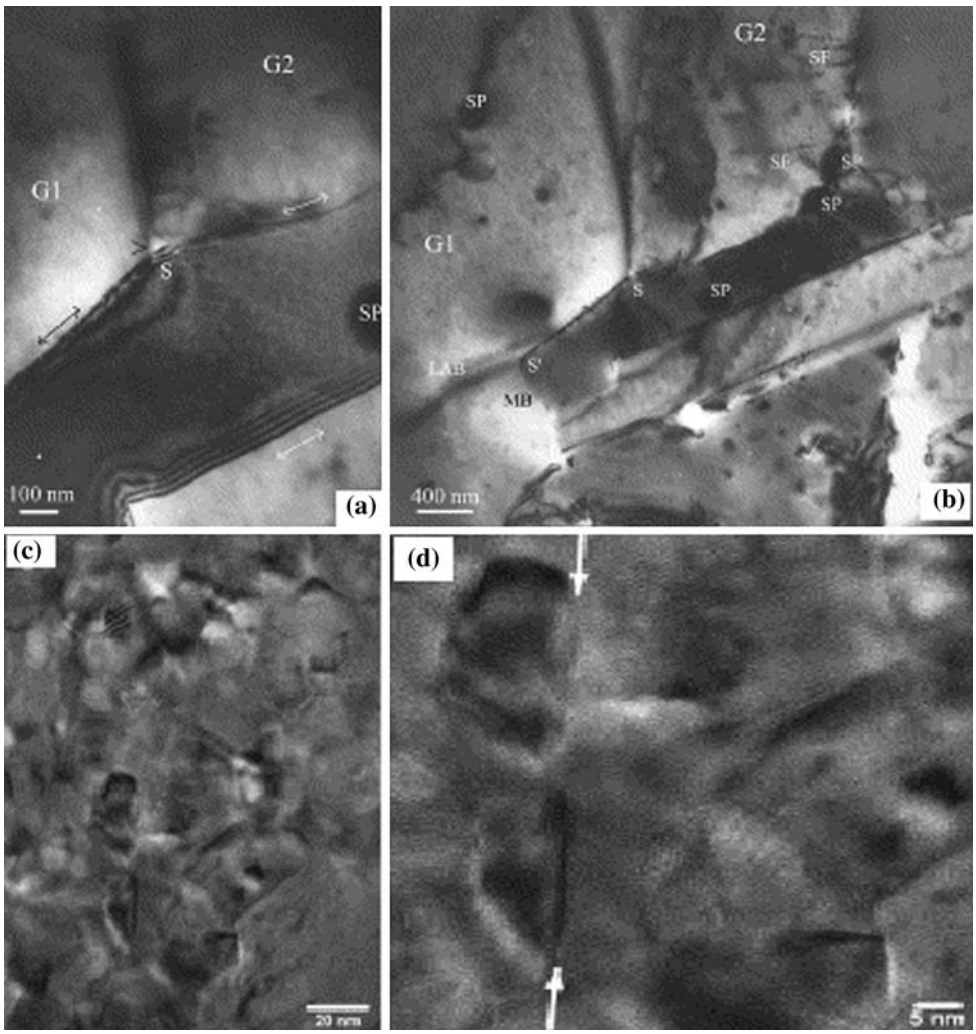

Fig. 2 Electron micrographs showing **a** general direction of plausible grain boundary sliding (*double-headed arrow*); **b** deformation characteristics of the surrounding grains in the region and the change in the dihedral angle at a triple junction (after Ref. [122]); **c** high-resolution TEM micrograph of nanocrystalline Pd after rolling that shows nearly equi-axed grains, **d** enlarged section of (**c**), showing a mesoscopic shear plane extending over several grain boundaries (*arrowed*) (after Ref. [70])

Having established a case (a) for grain boundary sliding-diffusion coupled flow, and (b) development of mesoscopic boundary sliding during superplastic deformation, it is necessary to justify the assumption that dislocation motion does not contribute independently to superplastic deformation.

Quantitative texture analysis gives a clear idea about the thermo-mechanical history of a material and hence is useful in deciding if crystal deformation by dislocation motion is present as an independent mechanism during optimal superplastic flow or not [105, 106]. For this analysis [69] also, grains are assumed, as in the analysis for mesoscopic boundary sliding, to form an assembly of non-deforming quasi-rigid (near) spherical crystals surrounded by boundaries in three dimensions that flow in a viscous manner.

Such a description would suggest that as grain boundary shear stresses are non-zero and unbalanced, grain rotation will be facilitated. But as boundary sliding, which develops to a mesoscopic scale, is the rate-controlling step, grain rotations will be present as a non-rate controlling process to the extent needed to move boundaries of high viscosity away from the direction of propagation of the plane interface. As this will be a random process, a conclusion is reached that superplastic deformation in a material of initial isotropic microstructure will be isotropic. Many MD simulation studies of the grain boundary deformation process have in fact concluded that only evidence for grain boundary sliding and grain rotation could be obtained in an unambiguous manner [107–114]. Some of these papers have also suggested specifically that their observations are in accordance with our physical description (see, e.g., the two papers cited as Refs. [107, 108]). This prediction about the isotropic deformation of a material of initial isotropic microstructure has also been verified at the macro-level by testing cylindrical specimens with an equi-axed microstructure and random crystallographic orientation. Then, even after several hundred percent elongation, the cylindrical shape of the specimen was retained [1–3, 105].

From a theoretical point of view, the following statements can be made. (a) Random grain boundary sliding cannot cause any systematic change in the crystal

orientations and, consequently, that process cannot, on average, alter the texture. (b) Crystal/grain rotation, which will arise because of unbalanced shear stresses at the boundaries, will only weaken the existing texture, without changing the overall crystal orientations. (c) Grain rotations will be absent if diffusion were rate controlling and the boundary shear stresses are assumed to die down to zero instantaneously as in, e.g., the model presented in Ref. [64].

In Fig. 3, the "ghost-corrected" true orientation distribution function (ODF) plots of the superplastic alloy, Supral 100 (Al–6Cu–0.4Zr), are presented. Figure 3a corresponds to the grip portion of the tensile specimen, which was soaked at the test temperature of 730 K for the duration of the test and corresponds to the starting condition. Figure 3b is the ODF plot of a specimen deformed by 9.2% at room temperature. The texture changes here could be understood unambiguously as due to Taylor dislocation slip. In contrast, Fig. 3c and d correspond to the ODFs of specimens superplastically deformed to 175% (true strain $\simeq 1$) and 660% (true strain $\simeq 2$) elongation at 730 K. It is seen that with increasing superplastic deformation the texture peak present in the initial crystallite orientation distribution decays continuously, with a simultaneous broadening of the peak. As required when (nearly) random grain/interphase boundary sliding is rate controlling, no new texture peaks are introduced even after 660% elongation of the specimen. The decay in the texture

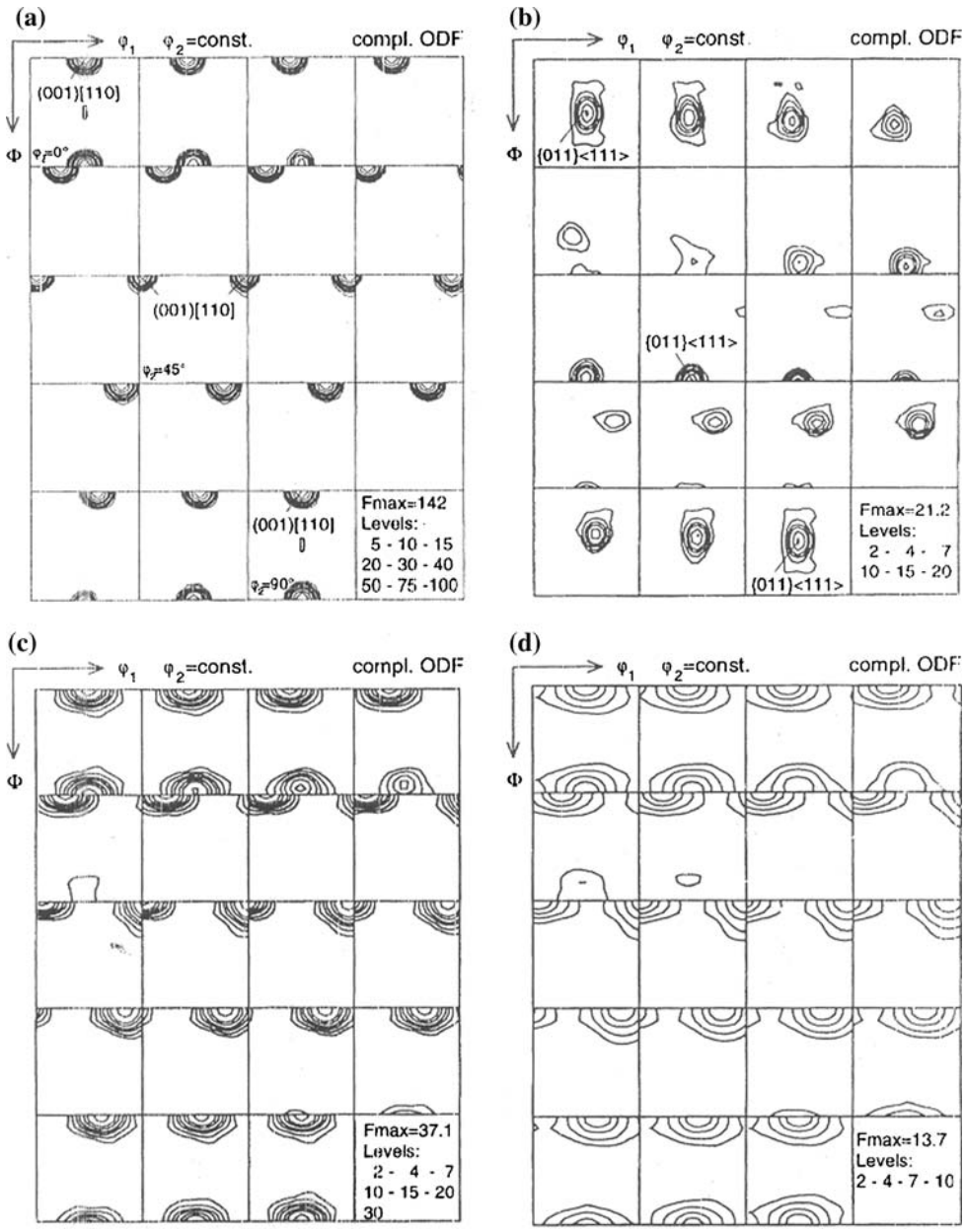

Fig. 3 Examples of the texture present at different stages of deformation: **a** undeformed state (grip section, soaked at 730 K); **b** deformed by 9.2% at room temperature; **c** deformed by 175% at 730 K ($\varepsilon \simeq 1$); **d** deformed by 660% at 730 K ($\varepsilon \simeq 2$) (after Ref. [69])

intensity with superplastic strain could be compared with the decay in the concentration with time in the diffusion couple problem in a straightforward manner (with superplastic strain replacing time and texture intensity taking the place of chemical concentration) to predict accurately the changes in the texture intensity with superplastic strain [69].

Mathematical development of the above-mentioned ideas has led to the following rate equation [71, 72].

$$\dot{\gamma}_{sp} = A(\tau_{sp} - \tau_0)\exp\left(\frac{\Delta F_0}{kT}\right);\ A = \left(\frac{2.0944W^4\gamma_0^2\nu}{kTL}\right) \quad (4)$$

where $\dot{\gamma}_{sp}$ is the shear strain rate, τ_{sp} the externally applied shear stress, τ_0 the long range threshold shear stress that should be overcome for the onset of mesoscopic boundary sliding, ΔF_0, the free energy of activation, which is given by Eq. 3, W is the grain boundary width $= 2.5a_0$, where a_0 is the diameter of the major atomic species in the material (the molecule in a ceramic), γ_0 the shear strain associated with the unit sliding event (=0.10), ν the thermal vibration frequency $= kT/h$ or 10^{13} s^{-1}, L the average grain size, k the Boltzmann constant, h the Planck constant and T is the temperature of deformation on the absolute scale. τ_0 in turn, is given by

$$\tau_0 = \left(\frac{8G\Gamma_B r}{3^{0.25}}\right)^{0.5}\left(\frac{1}{L}\right) \quad (5)$$

where Γ_B is the specific grain boundary energy and r is the average residual misfit at the grain boundary that is removed by diffusion.

An examination of Eq. 4 reveals that $\dot{\gamma}_{sp}(=\sqrt{3}\dot{\varepsilon}$ where $\dot{\varepsilon}$ is the measured external tensile strain rate) $-$ $\tau_{sp}(=\sigma/\sqrt{3})$, where σ is the externally applied tensile stress) pairs obtained experimentally for each system at several stress levels may be punched in and the unknown values of ΔF_0 and $\tau_0(=\sigma_0/\sqrt{3})$, where σ_0 is the tensile threshold stress that should be overcome for the onset of mesoscopic boundary sliding, can be obtained by a method of iteration, as explained later.

The procedure for solving the transcendental equation (4) also evolved over a few papers [71, 72, 115, 116]. Initially, "a brute force method" was adopted to solve a more complicated form of Eq. 4 (see Eq. 1 of Ref. [115]), which was derived for the same process when the internal stress distribution arising from atomic scale boundary sliding was assumed to be log normal in nature (an assumption which has since been dispensed with using better analytical procedures). The four unknown constants of the rate equation for isothermal flow and the activation energy for the rate-controlling process were determined using the method of least squares. In Ref. [116], a mathematical procedure to reduce the number of unknowns from 4 to 3 by suitably combining them and also to determine the stress at which the strain-rate sensitivity index, m, reaches its maximum value is presented. As this method reduces the superplastic rate equation up to the point of inflection in the $\ln\sigma - \ln\dot{\varepsilon}$ curve to a quadratic equation, a neat analytical solution for the unknowns is possible. In Ref. [71], by a simplification of the mathematical procedure, the rate equation is reduced to a transcendental equation involving three unknowns (see Eq. 18 of Ref. [71]). Then, the three unknowns were determined by the method of least squares. The present Eq. 4 was derived in Ref. [72]. In that equation, the following numerical values will apply for all systems under the categories of metals and alloys, ceramics, intermetallics and nanostructured materials, regardless of whether the grain size is in the micrometer, sub-micrometer, or nanometer range: $W = (2.5a_0)$, where a_0 is the atomic diameter of the species that has the maximum concentration in the alloy (or of the molecule in a ceramic), $\gamma_0 = \sqrt{3}$ $\varepsilon_0 = 0.10$, $\nu = 10^{13}s^{-1}$ or (kT/h), k is Boltzmann's constant, h is Planck's constant, T the absolute temperature of deformation and L the average grain size are defined by the testing conditions, $\dot{\gamma}_{sp}(=\sqrt{3}\dot{\varepsilon})$ and $\tau_{sp}(=(\dot{\varepsilon}/\sqrt{3}))$ are the observed shear strain rate and shear stress values (with $\dot{\varepsilon}$ and σ being their tensile/compressive counter parts), which are experimentally measured.

Therefore, there are only two unknowns: the free energy of activation for the rate controlling process, ΔF_0, and the tensile/compressive threshold stress, which has to be overcome for the onset of mesoscopic boundary sliding. To determine these two values, all that is needed are the $\sigma - \dot{\varepsilon}$ experimental values at a minimum of three temperatures. Then, using the two physical constraints imposed by the model, viz., (a) that σ_0, which is temperature-dependent should be less than σ_{min}, the minimum stress value at which flow is measured in the experiments, and (b) that ΔF_0 is independent of temperature, and the method of least squares, one can obtain these two unknowns uniquely from the experimental results. A more detailed description of this procedure will be presented elsewhere.

Following this procedure, experimental data concerning many metallic alloys, ceramics, nanostructured materials and intermetallics were analyzed [67, 71, 72]. The agreement between the theoretical and the experimental values was very good in all cases. Results pertaining to a few systems are presented in Tables 1, 2, 3 and Fig. 4.

Concluding remarks

As some may see a resemblance between our physical description, first conjectured in 1970 [57] and presented in detail in 1977 [59] on the one hand and the "core and

Table 1 Initial grain size 7.6 μm (after Ref. [71])

Temperature, T (K)	Observed stress, σ (MPa)	Observed strain rate, $\dot{\varepsilon}_{spobs}$ ($\times 10^5$ s^{-1})	Predicted strain rate, $\dot{\varepsilon}_{sppre}$ ($\times 10^5$ s^{-1})
793	0.70	2.5	1.6
	1.51	10.0	7.3
	2.35	19.0	13.0
	3.38	32.0	20.0
753	0.93	0.73	1.0
	2.04	3.7	3.5
	3.16	7.6	6.0
	4.05	11.0	8.0
713	2.16	0.79	1.1
	3.16	1.7	1.7
	4.17	3.5	2.3
	5.34	5.4	3.1
	5.87	6.1	3.4

Al–33.6wt.%Cu–0.44wt.% Zr (experimental data from Ref. [119])

mantle" model of Gifkins, presented in 1976 [117] on the other hand, there is a need to dispel that belief. In the "core and mantle" description, the widths of both the core and the mantle are assumed to change with the experimental conditions. As a result, two important physical parameters, viz., grain boundary width and activation energy for the rate-controlling process, are converted into adjustable parameters [105]. For example, the magnitude of activation energy for rate-controlling process is allowed to vary between 0.2 Q_l to 0.6 Q_l, in the optimal range and up to Q_l at high strain rates, where Q_l is the activation energy for the lattice diffusion. In contrast, in the present model, both grain boundary width (=2.5a_0) and the activation energy for grain boundary sliding (Eq. 3) have fixed/unique values and these values are consistent with experimental observations. Other shortcomings of the 'core and mantle' model are pointed out in Ref. [105] and the criticisms of a few others are collated in Ref. [1].

Likewise, some may see a similarity between our proposals for mesoscopic boundary sliding and plane interface formation (first presented in 1993 [65, 66]) on the one hand and those of Ovid'ko et al. [102, 103] presented in 2004/05. In the latter model, the gradual flattening of a triple junction is due to passage of appropriate grain boundary dislocations through triple junctions after gliding along high-angle boundaries. As noted in the section "Assumption and its justification", in contemporary view dislocations are not stable in general high-angle grin boundaries and a description of grain boundary sliding in terms of glide of grain boundary dislocations along such boundaries is not consistent with the different models of high-angle grain boundary presented since 1977 [85–96]

Table 2 Initial grain sizes in the range of 0.41–1.20 μm (after Ref. [71])

Temperature, T (K)	Grain size, L (μm)	Observed stress, σ (MPa)	Observed strain rate, $\dot{\varepsilon}_{spobs}$ ($\times 10^6$ s^{-1})	Predicted strain rate, $\dot{\varepsilon}_{sppre}$ ($\times 10^6$ s^{-1})
1723	1.2	3	0.14	3.77
		6	0.57	9.2
		16	4.1	27
		59	50	110
		96	160	170
		215	490	400
	0.66	3	0.22	0.10
		6	1.7	1.4
		20	21	61
		58	300	190
		98	720	320
		235	2200	800
	0.41	3	0.4	0.16
		6	2.6	16
		10	9.8	38
		16	40	70
		30	310	150
		39	790	190
		58	1200	300
		100	3200	530
		120	13000	1300
1673	0.41	6	0.46	7.1
		16	14	31
		42	290	93
		100	2000	230
		227	6000	600
1623	0.41	6	0.2	2.97
		20	3.9	1.7
		42	85	39
		100	540	98
		230	2000	230

ZrO_2 + 3 mol.% Y_2O_3 (experimental data from Ref. [120])

Table 3 Initial grain size 55 nm (after Ref. [71])

Temperature, T (K)	Observed stress, σ (MPa)	Observed strain rate, $\dot{\varepsilon}_{spobs}$ ($\times 10^6$ s^{-1})	Predicted strain rate, $\dot{\varepsilon}_{sppre}$ ($\times 10^6$ s^{-1})
1333	14.51	2.6	0.69
	17.14	4.9	1.3
	24.63	15	3.2
	52.09	31	10

ZrO_2 + 5 mol.% Y_2O_3 (experimental data from Ref. [121])

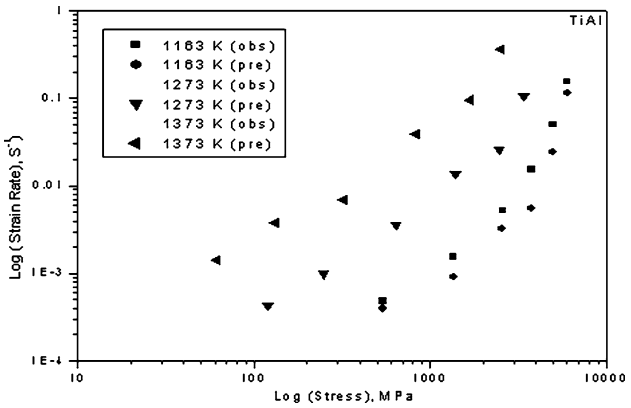

Fig. 4 Experimental and computed log strain rate–log stress plots at different temperatures in a TiAl intermetallic of a fixed initial grain size at all test temperatures (Padmanabhan KA, Basaria MR, unpublished work)

and also the MD simulation results. Our views on the physical process that underlies grain boundary sliding, where the expansion present in the high-angle grain boundary (compared with the crystal lattice) is described in terms of a free volume, are given in Refs. [65–67, 71, 72] and are summarized in the section "The analysis".

The present model is different from the others presented so far on grain boundary sliding in that it arrives at a strain rate equation for this process, per se, by treating it to be the rate-controlling mechanism rather than suggesting that it is a faster, accommodation process and that the rate of deformation is attributable to the other mechanism. Starting from this viewpoint two important predictions were made: (a) that the boundary sliding process will develop to a mesoscopic scale and that will lead to plane interface formation (first predicted in 1993 [65, 66]) and (b) that as boundary sliding rate control ensures the presence of unbalanced shear stresses, (near-) random grain rotation will be present and this will lead to a gradual reduction in the texture intensity with superplastic strain, without the appearance of new texture peaks [69, 106]. Experimental support for these predictions is available (see Figs. 2 and 3).

With regard to numerical agreement between the experimental observations and the calculations based on Eq. 4, one could say the following: (a) For all systems pertaining to the different classes of metals and alloys, ceramics, intermetallics and nanostructured materials, when the grain size lies in the micrometer to nanometer range, one could assume in Eq. 4, $W = (2.5a_0)$, $\gamma_0 = \sqrt{3}\,\varepsilon_0 = 0.10$, $\nu = 10^{13}\,\mathrm{s}^{-1}$ or (kT/h), with k the Boltzmann constant and h the Planck constant. If from superplasticity experiments the $\dot{\varepsilon}$ and σ data pairs for at least three temperatures are known, along with the value of the average grain size, using the same Eq. 4 one could determine the values of ΔF_0, and σ_0, without any external inputs, using the method of iteration described earlier. (b) When the transcendental strain rate equation was solved, with three unknowns [71]—see Tables 1, 2 and 3—the strain rate could be predicted in most cases within a factor of 4 of the experimental values. This numerical factor could be reduced to 2, with the latest method of solving Eq. 4 described earlier. Very recently, using this method high-strain rate superplastic deformation was analyzed. Here again, the accuracy of the fit could be ensured to remain within a factor of 2. These results will be reported elsewhere. It is pertinent to note in this regard that in such order of magnitude calculations, the accuracy of prediction is said to be good, when the calculated value is within a factor of 10 of the experimental value.

The next step is to extend the deformation process described to macroscopic level using Finite Element Analysis. Typical problems of interest could be (a) the length of the plane interface formed by mesoscopic sliding as a function of grain size, stress, and temperature; (b) determination of non-uniform stress distribution that develops through grain boundary sliding at the microstructural and mesoscopic levels (as in the present description, the 3D grain boundary network forms an infinite continuum).

Moreover, an examination of Eq. 3 reveals that if the shear modulus, G, in the grain boundary region of a material is known at different temperatures, it will then be possible to predict using the ΔF_0 value already obtained the free volume that would be present in the high-angle grain boundary at different temperatures. This can then be verified by molecular dynamics (MD) simulations. Likewise, from Eq. 5, one can obtain the value of r, the average misfit removed by diffusion from the high-angle boundary at a given temperature, if the value of G and the specific grain boundary energy, Γ_B (again computable by MD simulations [118]), for the material at that temperature are known. Thus, there is scope for validating this model down to the level of MD simulations.

The idea of stress-directed movement of free volume along a grain boundary/interface used in this analysis can apply equally well while interpreting superplastic deformation in bulk metallic glasses [125]. An investigation along these lines would be worthwhile.

References

1. Padmanabhan KA, Davies GJ (1980) Superplasticity. Springer-Verlag, Heidelberg, Berlin
2. Kaibyshev OA (1992) Superplasticity in alloys, intermetallides and ceramics. Springer-Verlag, Heidelberg, Berlin
3. Nieh TG, Wadsworth J, Sherby OD (1997) Superplasticity in metals and ceramics. Cambridge University Press, Cambridge

4. Mishra RS, Stolyarov VV, Esher C, Valiev RZ, Mukherjee AK (2001) Mater Sci Eng A 298:44
5. Islamgaliev RK, Valiev RZ, Mishra RS, Mukherjee AK (2001) Mater Sci Eng A 304–306:206
6. McFadden SX, Valiev RZ, Mukherjee AK (2001) Mater Sci Eng A 319–321:849
7. Sergueeva AV, Stolyarov VV, Valiev RZ, Mukherjee AK (2002) Mater Sci Eng A 323:318
8. Dobatkin SV, Bastarache EN, Sakai G, Fujita T, Horita Z, Langdon TG (2005) Mater Sci Eng A 408:141
9. Horita Z, Langdon TG (2008) Scr Mater 58:1029
10. Kai M, Horita Z, Langdon TG (2008) Mater Sci Eng A 488:117
11. Neishi K, Horita Z, Langdon TG (2001) Scr Mater 45:965
12. Komura S, Furukawa M, Horita Z, Nemoto M, Langdon TG (2001) Mater Sci Eng A 297:111
13. Furui M, Kitamura H, Anada H, Langdon TG (2007) Acta Mater 55:1083
14. Neishi K, Uchida T, Yamauchi A, Nakamura K, Horita Z, Langdon TG (2001) Mater Sci Eng A 307:23
15. Perevezentsev VN, Chuvil'deev VN, Kopylov VI, Syseev AN, Langdon TG (2002) Ann Chimie Sci Materiaux 27:99
16. Figueiredo RB, Kawasaki M, Xu C, Langdon TG (2008) Mater Sci Eng A 493:104
17. Malek P, Turba K, Cieslar M, Drbohlav I, Kruml T (2007) Mater Sci Eng A 462:95
18. Musin F, Kaibyshev R, Motohashi Y, Itah G (2004) Scr Metall 50:511
19. Watanabe H, Mukai T, Ishikawa K, Higashi K (2002) Scr Mater 46:851
20. Cavaliere P, De Marco PP (2007) Mater Sci Eng A 462:206
21. Cavaliere P, De Marco PP (2007) Mater Sci Eng A 462:393
22. Kim WJ, Park JD, Wang JY, Sakk WSYY (2007) Scr Mater 57:755
23. Wang Q, Wei Y, Chino Y, Mabuchi M (2008) Rare Met 27:719
24. Wei YH, Wang QD, Zhu YP, Zhou HT, Ding WJ, Chino Y, Mubuchi M (2003) Mater Sci Eng A 360:107
25. Zhang KF, Ding S, Wang GF (2008) Mater Lett 62:719
26. Kim WJ, Lee KE, Park J, Kim MG, Wang JY, Yoon US (2008) Mater Sci Eng A 494:391
27. Duclos R (2004) J Eur Ceram Soc 24:3103
28. Figueiredo FB, Langdon TG (2006) Mater Sci Eng A 430:151
29. Bate PS, Ridley N, Zhang B (2007) Acta Mater 55:4995
30. Valiev RZ, Islamgaliev RK, Semenova IP (2007) Mater Sci Eng A 463:2
31. Watanabe H, Mukai T, Mabuchi M, Higashi K (2001) Acta Mater 49:2027
32. Klassen T, Suryanarayana C, Bormann R (2008) Scr Metall 59:455
33. Hiraga K, Kim B-N, Morita K, Yoshida H, Suzuki TS (2007) Sci Technol Adv Mater 8:578
34. Morita K, Higara K, Kim B-N (2007) Acta Mater 55:4517
35. Kishimoto A, Obata M, Asaeka H, Haya H (2007) J Eur Ceram Soc 27:41
36. Xu X, Nishimura T, Hirosaki N, Xie R-J, Yamamoto Y, Tanaka H (2006) Acta Mater 54:255
37. Charit I, Chokshi AH (2001) Acta Mater 49:2239
38. Imai T, Mao J, Dang S, Shigematsu I, Saito N, L'Esperance G (2004) Mater Sci Eng A 364:281
39. Zhan G-D, Mitomo M, Xie R-J, Kurashima K (2000) Acta Mater 48:2373
40. Zhou X, Hulbert DM, Kuntz JD, Sadangi RK, Shukla V, Kear BH, Mukherjee AK (2005) Mater Sci Eng A 394:353
41. Chen T, Mohamed FA, Mecartney ML (2006) Acta Mater 54:4415
42. Blandin J-J, Dendievel R (2000) Acta Mater 48:1541
43. Morita K, Hiraga K (2003) Scr Metall 48:1403
44. Kaibyshev OA, Pshenichnyuk AI (2005) Mater Sci Eng A 410–411:105
45. Muto H, Sakai M (2001) Acta Mater 48:4161
46. Yasuda K, Okamoto T, Shiota T, Matsuo Y (2006) Mater Sci Eng A 418:115
47. Balasubramanian N, Langdon TG (2003) Scr Mater 48:599
48. Balasubramanian N, Langdon TG (2005) Mater Sci Eng A 409:46
49. Chokshi AH (2002) J Eur Ceram Soc 22:2469
50. Padmanabhan KA, Vasin RA, Enikeev FU (2001) Superplastic flow: phenomenology and mechanics. Springer-Verlag, Heidelberg, Berlin
51. Mukherjee AK (2002) Mater Sci Eng A 322:1
52. Zhu YT, Langdon TG (2005) Mater Sci Eng A 409:234
53. Brown AM, Ashby MF (1980) Scr Metall 14:1297
54. Stocker RL, Ashby MF (1973) Scr Metall 7:115
55. Derby B, Ashby MF (1984) Scr Metall 18:1079
56. Pharr GM (1985) Scr Metall 19:1347
57. Davies GJ, Edington JW, Cutler CP, Padmanabhan KA (1970) J Mater Sci 5:1091. doi:10.1007/BF00553897
58. Padmanabhan KA (1971) Some aspects of superplasticity in metals. University of Cambridge, UK
59. Padmanabhan KA (1977) Mater Sci Eng 29:1
60. Speight MV (1975) Acta Mater 23:779
61. Speight MV (1976) Scr Metall 10:163
62. Stevens RN (1971) Philos Mag 23:265
63. Cannon WR (1972) Philos Mag 25:1489
64. Ashby MF, Verrall RA (1973) Acta Metall 21:149
65. Padmanabhan KA, Schlipf J (1993) In: Guceri SI (ed) Proceedings of the first international conference on transport phenomena in processing. Technomic Publishing Co., Lancaster, PA, p 491
66. Padmanabhan KA, Schlipf J (1996) Mater Sci Technol 12:391
67. Hahn H, Padmanabhan KA (1997) Philos Mag B 76:559
68. Hahn H, Mondal P, Padmanabhan KA (1997) Nanostruct Mater 9:603
69. Engler O, Padmanabhan KA, Luecke K (2000) Model Simul Mater Sci Eng 8:477
70. Markmann J, Bunzel P, Roesner H, Liu KW, Padmanabhan KA, Birringer R, Gleiter H, Weissmueller J (2003) Scr Mater 49:637
71. Padmanabhan KA, Gleiter H (2004) Mater Sci Eng A 381:28
72. Padmanabhan KA, Dinda GP, Hahn H, Gleiter H (2007) Mater Sci Eng A 452–453:462
73. Bhattacharya SS, Padmanabhan KA (1989) Trans Ind Inst Met 42(Suppl):5123
74. Gittus JH (1975) Creep, viscoelasticity and creep fracture in solids. Applied Science Publishers, London, p 18
75. Biscondi M, Goux C (1968) Mem Sci Rev Met 65:167
76. Wadsworth J, Palmer IG, Crooks DD, Lewis RE (1983) In: Starke ES Jr, Sandoss TH Jr (eds) Proceedings of the second international Al-Li conference. Met. Soc. AIME, Warrendale, p 111
77. Kronberg ML, Wilson FH (1949) Trans Am Inst Min Metall Engrs 185:501
78. Read WT, Shockley W (1950) Phys Rev 78:275
79. Brandon DG, Ralph B, Ranganathan S, Wald MS (1964) Acta Metall 12:813
80. Christian JW, Crocker AG (1980) In: Nabarro FRN (ed) Dislocations in solids, vol 3. North Holland Publishing Co., Oxford, p 165
81. Pumphrey PH, Gleiter H (1974) Philos Mag 30:593
82. Pumphrey PH, Gleiter H (1975) Philos Mag 32:881
83. Bullough R, Tewari VK (1979) In: Nabarro FRN (ed) Dislocations in solids, vol 2. North Holland Publishing Co., Oxford, p 1
84. Bollmann W, Michaut B, Sainfort G (1972) Phys Stat Sol (a) 13:13

85. Smith DA, Vitek V, Pond RC (1977) Acta Metall 25:475
86. Pond RC, Smith DA (1977) Philos Mag 36:353
87. Pond RC, Smith DA, Vitek V (1978) Scr Metall 12:699
88. Ashby MF, Spaepen F (1978) Scr Metall 12:193
89. Ashby MF, Spaepen F, Williams S (1978) Acta Metall 26:1647
90. Sutton AP, Vitek V (1980) Scr Metall 14:129
91. Sutton AP, Vitek V (1980) In: Ashby MF et al (eds) Proceedings of the international conference on dislocation modelling of physical systems. Pergamon, Oxford, p 549
92. Sutton AP, Baluffi RW, Vitek V (1981) Scr Metall 15:989
93. Sutton AP (1982) Philos Mag A 46:171
94. Sutton AP, Vitek V (1983) Philos Trans R Soc A 309:1, 37, 55
95. Schwartz D, Vitek V, Sutton AP (1985) Philos Mag A 51:499
96. Wolf D (1990) Acta Metall Mater 38:781, 791
97. Eshelby JD (1957) Proc Roy Soc A 241:376
98. Haasen P (1978) Physical metallurgy. Cambridge University Press, Cambridge, pp 46–47
99. Van Swygenhoven H, Frakas D, Caro A (2000) Phys Rev B 62:831
100. Perevezentsev VN, Rybin VV, Chuvildeev VN (1992) Acta Metall Mater 40:895
101. Sergueeva AV, Mara NA, Valiev RZ, Mukherjee AK (2005) Mater Sci Eng A 410–411:413
102. Gutkin MYu, Ovid'ko IA, Skiba NV (2004) Acta Mater 52:1711
103. Ovid'ko IA, Sheinerman AG (2005) Acta Mater 53:1347
104. Kaibyshev OA (2002) Mater Sci Eng A 324:96
105. Edington JW, Melton KN, Cutler CP (1976) Prog Mater Sci 21(2):63
106. Padmanabhan KA, Luecke K (1986) Z Metallkd 77:765
107. Swygenhoven HV, Caro A (1997) Appl Phys Lett 71:1652
108. Swygenhoven HV, Caro A (1997) Nanostruct Mater 9:669
109. Schiotz J, DiTollo FD, Jacobsen KW (1998) Nature 391:561
110. Swygenhoven HV, Caro A (1998) Phys Rev B 58:11246
111. Swygenhoven HV, Spaczer M, Caro A, Farkas D (1999) Phys Rev B 60:22
112. Schiotz J, Vegge T, DiTillo FD, Jacobsen KW (1999) Phys Rev B 60:11971
113. Swygenhoven HV, Spaczer M, Caro A (1999) Acta Mater 47:3117
114. Swygenhoven HV, Derlet P (2001) Phys Rev B 64:4105
115. Venkatesh TA, Bhattacharya SS, Padmanabhan KA, Schlipf J (1996) Mater Sci Technol 12:635
116. Enikeev FU, Padmanabhan KA, Bhattacharya SS (1999) Mater Sci Technol 15:673
117. Gifkins RC (1976) Metall Trans 7A:1225
118. Keblinski P, Wolf D, Phillpot SR, Gleiter H (1999) Scr Metall Mater 41:631
119. Matsuki K, Minami K, Tokizawa M, Murakami Y (1979) Met Sci 13:619
120. Owen DM, Chokshi AH (1998) Acta Mater 46:667
121. Betz U, Padmanabhan KA, Hahn H (2001) J Mater Sci 36:5811. doi:10.1023/A:1012956005571
122. Gouthama, Padmanabhan KA (2003) Scr Mater 49:761
123. Astanin VV, Faizova SN, Padmanabhan KA (1996) Mater Sci Technol 1:489
124. Mara NA, Sergueeva AV, Mara TD, McFadden SX, Mukherjee AK (2007) Mater Sci Eng A 463:238
125. Inoue A (2000) Acta Mater 48:279